Sensing and Control of MEMS Accelerometers Using Kalman Filter

Lili Dong[1], Kai Zhang[1]

1. Department of Electrical and Computer Engineering, Cleveland State University, Cleveland, OH 44115, USA
E-mail: L.Dong34@csuohio.edu

Abstract: A Kalman filter is designed and implemented for a MEMS capacitive accelerometer in order to filter out two major noise sources in the accelerometer, which are electronic noise and thermal mechanical noise (Brown noise). The dynamic modeling of the MEMS accelerometer is developed. A Kalman filter based force-to-rebalance controller is constructed on the model. Simulation results show that the Kalman filter based controller produces an excellent noise reduction, increases the dynamic range of the accelerometer, and stabilizes the accelerometer system under a closed-loop structure.

Key Words: MEMS accelerometer, Kalman filter, force-to-rebalance control, electronic noise, thermal mechanical noise.

I. INTRODUCTION

Micro-Electro-Mechanical Systems (MEMS) integrate mechanical transducers with electrical circuits. They have been broadly applied to various fields such as automotives, bio-medical area, and military system. Inertial MEMS sensors including MEMS accelerometers and gyroscopes occupy more than 20% of MEMS market. MEMS accelerometers alone have the second largest sales volume after pressure sensors. As an acceleration and deceleration sensor, MEMS accelerometers have been extensively applied to airbag deployment systems in automobiles [1]. This paper focuses on two fundamental problems of MEMS accelerometers: sensing and control.

Capacitive sensing mechanism has the advantages of low power dissipation, low cost, and low temperature coefficients [1]. Therefore, we construct controller based on micro-machined capacitive accelerometers. The Brownian noise caused by damping effect and the electronic noise from CMOS readout circuits are two major noise sources in capacitive accelerometers. Besides noise, the sensing accuracy of a micro-machined accelerometer is also limited by the nonlinearities and system uncertainties due to fabrication imperfections. Therefore, a feedback controller is essential for an accelerometer to compensate for the fabrication imperfections and to improve its performance. Specifically we need to design a controller that can reduce the offsets caused by mechanical imperfections and increase the bandwidth, sensitivity and dynamic range of accelerometers.

Currently, most MEMS products use open-loop control method instead of closed-loop control due to their space limit and their low requirements for dynamic range. The complication and high cost of closed-loop operation also limit its use. However, compared to open-loop control method, closed-loop control is more robust against noise and external disturbances. Two major closed-loop control methods are applied to capacitive accelerometers. They are force-to-rebalance closed-loop control [2-6] and a compensator based $\Delta\Sigma$ loop control [7-10]. Force-to-rebalance closed-loop control has been broadly used in MEMS inertial sensors for decades. It is successfully applied in Analog Devices' recent ADXL series MEMS accelerometers. The force-to-rebalance control is generally based on the analog signals output from an accelerometer. It can provide fast and real-time control signal to the sensor. A $\Delta\Sigma$ loop with feed-back compensator has been introduced in [7-10]. The $\Delta\Sigma$ modulators are also called over-sampling Analog to Digital converters, in which a digital signal has higher noise immunity than that of analog signal. However, the processing time of digital signals could be lengthy, making the control system not real-time.

In this paper, we investigate MEMS capacitive accelerometers with switch capacitive sensing and force-to-rebalance control strategy. Our goal is to reduce the noise in the accelerometer while keeping its good sensing performance through a close-loop control system. Our method is to use the Kalman filter as an observer to estimate the states of accelerometer through measured outputs, and then employ the estimated states which have much lower noise influence to close the system. This method not only gives a noiseless estimated output, but also improves the control performance.

The rest of this paper is organized as follows. The dynamic modeling of the MEMS accelerometer is given in section II. The noise in MEMS accelerometers is discussed in Section III. The design of Kalman filter based force-to-rebalance control is developed in section IV. The simulation results are shown in section V. Section VI gives concluding remarks and suggests future research.

II. DYNAMIC MIDELING OF MEMES ACCELEROMETER

Accelerometer is a sensor that transfers an acceleration signal into an electronic signal such as voltage.

2.1. Modeling of Mechanical Structure

978-1-4577-2074-1/12/$26.00

The basic mechanical structure of a MEMS accelerometer is shown in Fig. 1.

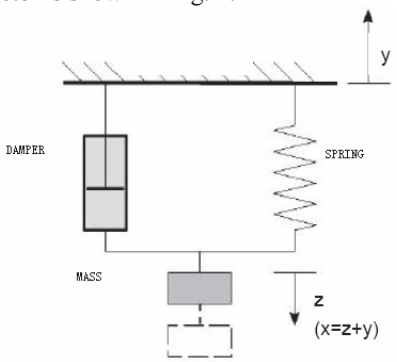

Fig. 1: Mechanical model of a MEMS accelerometer

In Fig. 1, after the acceleration is created along *y* direction, the mass will move a distance *x* which is a relative displacement between the mass and seismic base. The displacement of seismic base is *y*. Symbol *z* represents the absolute displacement of the mass. Following Newton's law, we obtain:

$$m\ddot{x}(t)+b\dot{x}(t)+kx(t)=m\ddot{y}(t)=ma(t) \tag{1}$$

where *m* is seismic mass, *b* is damping coefficient, *k* is spring constant and *a(t)* is acceleration. The transfer function (*H(s)*) between *a(s)* and *x(s)* can be written as:

$$H(s)=\frac{x(s)}{a(s)}=\frac{1}{s^2+\frac{b}{m}s+\frac{k}{m}} \tag{2}$$

We define the natural frequency ω_n and damping ratio ξ as

$$\omega_n=\sqrt{\frac{k}{m}},\qquad \zeta=\frac{b}{2\sqrt{km}} \tag{3}$$

We consider the under-damped situation. We suppose the accelerometer is designed to have a resonant frequency ω_n which is much larger than the maximum frequency of the acceleration signal. For a large ω_n, and a constant acceleration *a*, the quasi-static response is $x=a/(\omega_n^2)$. Therefore, the sensitivity of the accelerometer is given by

$$\frac{x(s)}{a(s)}=\frac{m}{k}=\frac{1}{\omega_n^2} \tag{4}$$

2.2. Modeling of CMOS Readout Circuit

The readout capacitor of a MEMS capacitive accelerometer is shown in Fig. 2 where there are two fixed electrodes and a movable seismic mass in the middle. A high frequency sinusoidal signal v_1 is added to the upper fixed electrode and an inversed signal v_2 is added to the lower fixed electrode. The signal v_B is bias voltage.

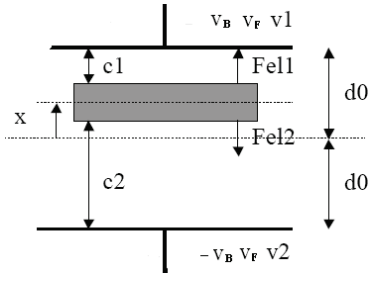

Fig. 2: Accelerometer capacitor

As show in Fig. 2, C_1 and C_2 are two variable sensing capacitors formed between the fixed electrodes and movable seismic mass, *x* is the relative displacement between seismic mass and fixed mass, and F_{el1} and F_{el2} are two opposite electrostatic forces. The fundamental readout circuit is shown in Fig. 3.

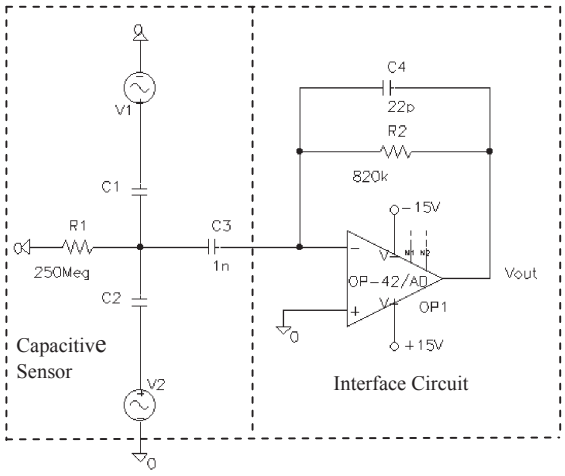

Fig. 3: Readout circuit of capacitor accelerometer [10]

Assuming the operational amplifier (OP-42/AD) in Fig.3 is ideal, we will obtain the output voltage V_o (or V_{out}) in Laplace transform as follows.

$$v_o(s)=-\frac{sC_3R_2}{1+sC_4R_2}\cdot\frac{v_1sC_1+v_2sC_2}{sC_1+sC_2+sC_3+1/R_1} \tag{5}$$

Suppose $C_1=C_0+\Delta C$, $C_2=C_0-\Delta C$, and $v_1=-v_2$, where C_o is the capacitance when the movable seismic mass is in the middle of two fixed plates, and ΔC is capacitance change caused by the movement of seismic mass. Equation (5) can be rewritten as

$$v_o(s)=-\frac{sC_3R_2}{1+sC_4R_2}\cdot\frac{2v_1s\Delta C}{sC_1+sC_2+sC_3+1/R_1} \tag{6}$$

Then assume $C_3>>C_1+C_2$, $1/R_1\approx 0$ and $sC_4R_2>>1$. Equation (6) can be simplified as

$$v_0(s)=-\frac{2\Delta C}{C_4}v_1(s) \tag{7}$$

Basing on a parallel-plate capacitor's formula, we have:

$$2\Delta C=C_1-C_2=\frac{2\varepsilon_0\varepsilon_r Ax}{(d_0^2-x^2)} \tag{8}$$

In (8), d_0 is the distance between fixed plate and movable seismic mass when the mass is in the middle, ε_0 is electric permittivity of vacuum, ε_r is relative dielectric constant and *A* is the area of the plate. Substituting (8) into (7) yields:

$$v_0(s)=-\frac{2\varepsilon_0\varepsilon_r Ax}{C_4(d_0^2-x^2)}v_1(s) \tag{9}$$

We assume $d_o >> x$. The output voltage v_o is given by

$$v_0(s)=-\frac{2\varepsilon_0\varepsilon_r Av_1(s)}{C_4d_0^2}x. \tag{10}$$

Therefore, we can detect the change of acceleration through measuring the output voltage v_o.

2.3. Modeling of Electrostatic Actuator

As the seismic mass is not in the middle, the electrostatic forces F_{el1} and F_{el} will take effect on the seismic mass. Since $v_1 = -v_2 = V_1 \sin \omega t$, we can obtain the total electrostatic force of the MEMS accelerometer as follows.

$$F_{el} = F_{el1} - F_{el2} = \frac{\varepsilon_0 \varepsilon_r A (V_1 \sin \omega t)^2}{2} \left(\frac{1}{(d_0 - x)^2} - \frac{1}{(d_0 + x)^2} \right) \tag{11}$$

The mechanical and electronic parameter values of a capacitive MEMS accelerometer are listed in Table I.

Table I: Parameters of a capacitive MEMS accelerometer

Area of seismic mass, A	$1200 \times 1550 \mu m$
viscosity of air, μ	$1.78 \times 10^{-5}\ kg/(m \times s)$
Seismic Mass, m	$3.8 \times 10^{-9} kg$
Gap, d_o	$2.3 \mu m$
Operation signal voltage, v_1	$0.6 volt$
Operation signal frequency, f	$1 MHz$
Spring coefficient, k	$3 Nm^{-1}$
Damping coefficient, b	$7 \times 10^{-4} kgs^{-1}$ (small deflection)
Relative dielectric constant, ε_r	4
Capacitor, C_4	$20 pF$

III. NOISE IN MEMS ACCELEROMETERS

Brownian noise and electronic noise are two main causes that degrade the performance of MEMS accelerometers.

3.1. Brown Noise

Brownian noise is thermal-mechanical noise. It creates a random force with Brownian motion of air molecules caused by damping. From [10], the power spectral density (PSD) of the Brownian noise force is

$$\overline{F_B^2}(f) = 4 k_B T b \tag{12}$$

where F_B is the Brownian noise force, k_B is Boltzman constant, T is absolute temperature, and b is damping coefficient. Brownian noise is a white noise which has a zero mean and $F_B{}^2$ variance.

3.2. Electronic Noise

In Fig. 3, there are three kinds of noises in interface circuit, which are MOSFET thermal noise, MOSFET flicker noise and diode leakage noise represented by $\overline{v_{ntherm}^2}(f)$, $\overline{v_{nflicker}^2}(f)$ and $\overline{v_{nleak}^2}(f)$ respectively. The PSD of the total output noise voltage is

$$\overline{v_n^2} = \overline{v_{nthermal}^2}(f) + \overline{v_{nflicker}^2}(f) + \overline{v_{nleak}^2}(f). \tag{13}$$

With a constant circuit's operating frequency f, the noise voltage can be determined as a random noise with zero mean and variance of $\overline{v_n^2}$. Since electronic noise affects the measurement result of accelerometers, it is also considered as measurement noise.

3.3. Noise Performance in Open and Closed-loop Systems

Suppose we use a traditional PI controller to control the output voltage signal from accelerometer. The block diagram of a closed-loop accelerometer system is given in Fig. 4 where the Brownian noise F_B is added to the system input as a random force and the electronic noise V_N is added to the system output as a random voltage.

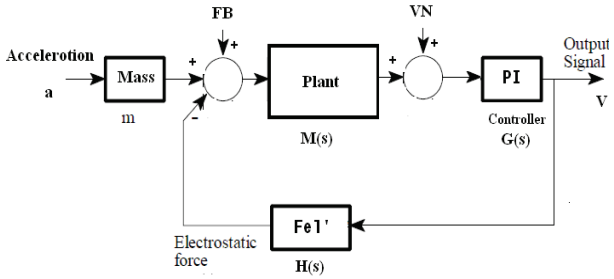

Fig. 4: Closed-loop accelerometer model with noises

In Fig. 4, PI controller can not control electrostatic force directly since the force is not measurable. However, voltage signal can be measured and used to create a feedback electrostatic force F_{el}'. The negative feedback force F_{el}' can compensate the seismic mass' displacement x which is created by input acceleration, and push the seismic mass back to the initial balanced middle position. Hence we also name the closed-loop system in Fig. 4 as force-to-rebalance control. We can get two signal-to-noise ratios (SNR) from Fig. 4. The *SNR (B)* between Brownian noise and acceleration and *SNR (E)* between electronic noise and acceleration are given by

$$SNR(B) = \frac{\dfrac{M(s)G(s)ma}{1 + H(s)M(s)G(s)}}{\dfrac{F_B M(s)G(s)}{1 + H(s)M(s)G(s)}} = \frac{ma}{F_B} \tag{14}$$

$$SNR(E) = \frac{\dfrac{M(s)G(s)ma}{1 + H(s)M(s)G(s)}}{\dfrac{V_N G(s)}{1 + H(s)M(s)G(s)}} = \frac{M(s)ma}{V_N} \tag{15}$$

The open-loop accelerometer model with Brownian and electronic noises is shown in Fig. 5 where the electrostatic force F_{el} is a part of the accelerometer plant. Voltage v_1 is the output signal of the accelerometer.

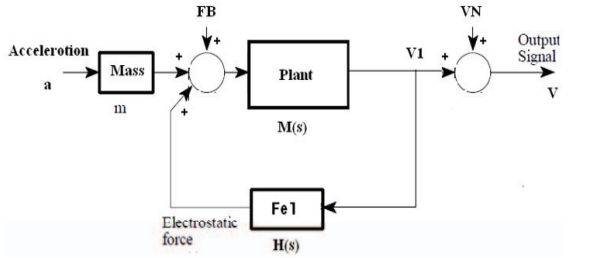

Fig. 5: Open-loop accelerometer model with noises

In Fig. 5, the SNRs for the open-loop system are given by

$$SNR(B) = \frac{M(s)ma}{M(s)F_B} = \frac{ma}{F_B} \tag{16}$$

$$SNR(E) = \frac{M(s)ma}{(1 - M(s)H(s))V_N} \tag{17}$$

From (14) to (17), we can see that the SNRs for Brownian noise are same for both open-loop and closed-loop systems. However, the *SNR (E)* of open-loop system is larger than that of closed-loop system. The noise performance of PI controlled closed-loop system is worse than the one for open-loop system. So a new control method has to be designed to replace PI controller.

IV. DESIGN OF A KALMAN FILTER BASED FORCE-TO-REBALANCE CONTROL

4.1. Design of Continuous-time Kalman Filter

Kalman Filter is an optimal observer based on a quadratic function of the estimation errors between real states and observed states [11]. Consider a continuous Linear Time Invariant (LTI) system in following equation:

$$\begin{aligned} \dot{x}(t) &= Ax(t) + Bu(t) + \omega(t) \\ y(t) &= Cx(t) + v(t) \end{aligned} \tag{18}$$

where *x(t)* is a system's state vector, *u(t)* is system's input, *y(t)* is system's output, *A*, *B*, and *C* are state, input and output matrices, *ω(t)* is process noise and *v(t)* is measurement noise.

Kalman filter is used to design a state observer to estimate the state *x(t)* by $\hat{x}(t)$, such that the cost function (given below) is minimized.

$$J_e = E[(x(t) - \hat{x}(t)^T (x(t) - \hat{x}(t))] \tag{19}$$

The dynamic equation of steady state Kalman Filter is

$$\begin{aligned} \dot{\hat{x}} &= A\hat{x} + Bu + K_k (y - \hat{y}) \\ \hat{y} &= C\hat{x} \end{aligned} \tag{20}$$

In (20), K_k is Kalman gain which is given by:

$$K_k = P_e C^T R^{-1} \tag{21}$$

where P_e is the positive definite solution of Riccati equation:

$$P_e A^T + A P_e - P_e C^T R^{-1} C P_e + Q = 0 \tag{22}$$

4.2. Design of Discrete-time Kalman Filter

A discrete-time system is described as

$$\begin{aligned} x_{(k+1)} &= F_{(k)} x_{(k)} + G_{(k)} u_{(k)} + w_{(k)} \\ y_{(k)} &= H_{(k)} x_{(k)} + v_{(k)} \end{aligned} \tag{23}$$

where $x_{(k+1)}$ is discrete-time state vector, $F_{(k)}$, $G_{(k)}$, and $H_{(k)}$ are discrete-time state, input, and output matrices, $\omega_{(k)}$ is the process noise and $v_{(k)}$ is the measurement noise. The signals $\omega_{(k)}$ and $v_{(k)}$ are white, zero-mean, uncorrelated white noise with covariance Q_k and R_k respectively. Matrix $F_{(k)}$ gives the relationship of the states from step time kT (T is sampling time and $T = t_k - t_{k-1}$) to step time $(k+1)T$. The mathematical expressions for $F_{(k)}$, $G_{(k)}$, and $H_{(k)}$ are given by

$$\begin{aligned} F_{(k)} &= e^{AT} \\ G_{(k)} &= \int_{t_k}^{t_{k-1}} e^{A(t-\tau)} B u(\tau) d\tau \\ H_{(k)} &= C \end{aligned} \tag{24}$$

4.3. Design of Extended Kalman Filter (EKF)

Both of the continuous-time and discrete-time Kalman filters introduced before are for LTI systems. However, in the real world, there are no absolutely linear dynamic systems or sensors. Therefore the EKF is developed in this section to estimate the states non-linear dynamic systems. Suppose we have a non-linear discrete-time system model:

$$x_k = f_{k-1}(x_{k-1}, u_{k-1}, w_{k-1}) \tag{25}$$

$$y_k = h_k(x_k, v_k) \tag{26}$$

The noises are $\begin{matrix} w_k \sim (0, Q_k) \\ v_k \sim (0, R_k) \end{matrix}$, (27)

where the process noise w_{k-1} and measurement noise v_k are assumed to be zero-mean, white and uncorrelated noises. The Taylor series expansion for (25) is

$$\begin{aligned} x_k &= f_{k-1}(\hat{x}_{k-1}^+, u_{k-1}, 0) + \left.\frac{\partial f_{k-1}}{\partial x}\right|_{\hat{x}_{k-1}^+} (x_{k-1} - \hat{x}_{k-1}^+) + \left.\frac{\partial f_{k-1}}{\partial \omega}\right|_{\hat{x}_{k-1}^+} \omega_{k-1} \\ &= F_{k-1} x_{k-1} + [f_{k-1}(\hat{x}_{k-1}^+, u_{k-1}, 0) - F_{k-1} \hat{x}_{k-1}^+] + L_{k-1} \omega_{k-1} \\ &= F_{k-1} x_{k-1} + \tilde{u}_{k-1} + \tilde{\omega}_{k-1} \end{aligned} \tag{28}$$

where $F_{k-1} = \left.\frac{\partial f_{k-1}}{\partial x}\right|_{\hat{x}_{k-1}^+}$. (29)

$L_{k-1} = \left.\frac{\partial f_{k-1}}{\partial w}\right|_{\hat{x}_{k-1}^+}$

In (28), we defined the $f_{k-1}(\hat{x}_{k-1}^+, u_{k-1}, 0) - F_{k-1}\hat{x}_{k-1}^+$ as known control signal $\tilde{u}_{k-1}$ and $L_{k-1} w_{k-1}$ as the noise signal $\tilde{\omega}_{k-1}$. The Taylor series expansion for output equation (26) is given by

$$\begin{aligned} y_k &= h_k(\hat{x}_k^-, 0) + (x_k - \hat{x}_k^-) + \left.\frac{\partial h_k}{\partial v}\right|_{\hat{x}_k^-} v_k \\ &= H_k x_k + [h_k(\hat{x}_k^-, 0) - H_k \hat{x}_k^-] + M_k v_k \\ &= H_k x_k + z_k + \tilde{v}_k \end{aligned} \tag{30}$$

where $H_k = \left.\frac{\partial h_k}{\partial x}\right|_{\hat{x}_k^-}$. (31)

$M_k = \left.\frac{\partial h_k}{\partial v}\right|_{\hat{x}_k^-}$

In (30), the measurement equation is defined based on both the known signal $z_k = h_k(\hat{x}_k^-, 0) - H_k \hat{x}_k^-$ and measurement noise $\tilde{v}_k = M_k v_k$. Combining (28) and (30), we obtain a linearized system model at each time step.

4.4. Design of Hybrid Extended Kalman Filter (EKF)

In this section, a hybrid EKF based on continuous-time dynamic system and discrete-time measurements is introduced. Suppose we have hybrid system equations as follows:

$$\begin{aligned} \dot{x}(t) &= Ax(t) + Bu(t) + L\omega(t) \\ y_{(k)} &= H_{(k)} x_{(k)} + v_{(k)} \end{aligned} \tag{32}$$

where $\begin{matrix} w(t) \sim (0, Q) \\ v_k \sim (0, R_k) \end{matrix}$. (33)

In (32), L represents the scalar matrix for process noise.

The initialized state and covariance are given by

$$\begin{aligned} \hat{x}_0^+ &= E(x_0) \\ P_0^+ &= E[(x_0 - \hat{x}_0^+)(x_0 - \hat{x}_0^+)^T] \end{aligned} \tag{34}$$

Computing the partial derivative matrices of dynamic equation produces

$$A = \left.\frac{\partial A}{\partial x}\right|_{\hat{x}_{k-1}^{+}} \qquad (35)$$

$$L = \left.\frac{\partial L}{\partial w}\right|_{\hat{x}_{k-1}^{+}}$$

The times update equations are

$$\dot{P} = AP + PA^T + LQL^T \qquad (36)$$

$$\dot{\hat{x}}(t) = A\hat{x}(t) + Bu(t)$$

We start this update with $\hat{x}(t) = \hat{x}_{k-1}^{+}$ and $P = P_{k-1}^{+}$. After integration we get $\hat{x}_k^{-} = \hat{x}$. Computing the partial derivative matrices of measurement equation yields

$$H_k = \left.\frac{\partial h_k}{\partial x}\right|_{\hat{x}_k^{-}} \qquad (37)$$

$$M_k = \left.\frac{\partial h_k}{\partial v}\right|_{\hat{x}_k^{-}}$$

Measurement-update equations are

$$K_k = P_k^{-} H_k^T (H_k P_k^{-} H_k^T + M_k R_k M_k^T)^{-1} \qquad (38)$$

$$\hat{x}_k^{+} = \hat{x}_k^{-} + K_k[y_k - h_k(\hat{x}_k^{-}, 0)] \qquad (39)$$

$$P_k^{+} = (I - K_k H_k) P_k^{-} \qquad (40)$$

The block diagram for hybrid Kalman filter observer is shown in Fig. 6, where ADC is analog/digital converter, and DAC is digital/analog converter.

4.5 Application of Hybrid EKF to MEMS Accelerometers

We use the hybrid EKF (given by (32) to (40)) to estimate the acceleration signal for MEMS accelerometers. The accelerometer model represented by (1) and (10) can be rewritten as the mathematical form (32), where

$$A = \begin{bmatrix} 0 & 1 \\ -k/m & -b/m \end{bmatrix} \qquad (41)$$

$$B = L = \begin{bmatrix} 0 \\ 1/m \end{bmatrix} \qquad (42)$$

$$H = \begin{bmatrix} \frac{2\varepsilon_0 \varepsilon_r A V_1}{C_4 d_0^2}, & 0 \end{bmatrix} \qquad (43)$$

The block diagram of the closed-loop control system with hybrid EKF based observer is given in Fig. 6, where the plant is the accelerometer model given by (32).

V. SIMULATION RESULTS

The hybrid EFK (given by (32)) is simulated on a MEMS accelerometer model in Matlab/Simulink. We choose sinusoidal acceleration input at the frequency of 10 *Hz* with thermal-mechanical noise. We choose 1z*MHz* as the operating frequency of the readout circuit with electronic noise at 0.02*g*. Fig. 7 and Fig. 8 show the voltage and displacement outputs of MEMS accelerometer in an open-loop configuration as the input acceleration's magnitudes are 0.1*g* and 1*g*. Figures 9 to 12 show the actual and estimated voltage outputs and actual and estimated displacements of hybrid EKF observer based closed-loop accelerometer system. A brief summary of the simulation results is given in Table II. From Table II, we can see that the output of EKF based closed-loop accelerometer system has much smaller SNR than that of open-loop system. Moreover, the maximum displacement of seismic mass for open-loop system is bigger than the one for EKF based closed-loop system. The larger displacement of mass in open-loop system could cause the movable mass to be pulled to fixed plate, causing the failure of operation.

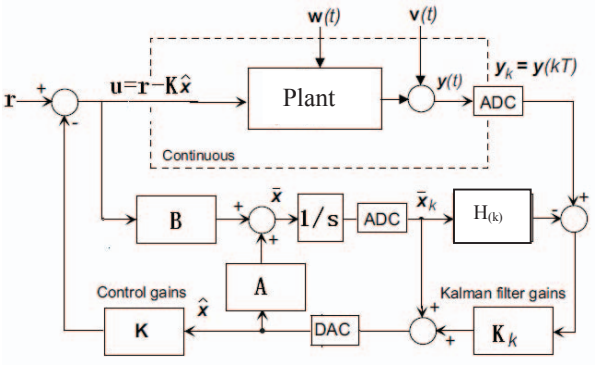

Fig. 6: Closed-loop control with hybrid EKF based observer

VI. CONCLUDING REMARKS

In this paper, a hybrid EKF based force-to-rebalance feedback control is originally applied to a capacitive MEMS accelerometer to improve its SNR and dynamic performance. Both mechanical thermal and electronic noises are considered in controller design. The MEMS accelerometer is simulated on open-loop and hybrid extended Kalman filter based closed-loop systems. The simulation results verified the effectiveness of the hybrid EKF. In the future, we plan to conduct hardware implementation of the hybrid EKF based controller on an actual MEMS accelerometer.

REFERENCES

[1]. Tai-Ran. Hsu, *MEMS & Microsystems: Design, Manufacture, and Nanoscale Engineering*, WILEY INTERSCIENCE, 2008.

[2]. J. Bernstein, "Low-Noise MEMS Vibration Sensor for Geophysical Application", *Journal of MEMS*, vol.8, no. 4, pp. 433-438, 1999.

[3]. G. Zhang, "Design and Simulation of a COMS-MEMS Accelerometer", M.S. Thesis, Dept. of Electrical and Computer Engineering (ECE), Carnegie Mellon University, 1998.

[4]. G.K. Fedder, "Simulation of Microelectromechanical System," Doctoral Dissertation, Department of Electrical Engineering and Computer Science, University of California at Berkeley, 1994.

[5]. T.Smith, "A 15*b* Electromechanical Sigma-Delta Converter for Acceleration Measurements," in *Proc. of IEEE Int. Solid-State Circuits Conf. Digest of Technical Papers*, San Francisco, CA, 1994, pp. 160-161.

[6]. K. H. Chau, S. Lewis, Y. Zhao, etc, "An Integrated Force-Balanced Capacitive Accelerometer for Low-G Applications," in *Proc. 8th Int. Conf. Solid-State Sensors and Actuators,* Stockholm, Sweden, June, 1995, pp. 593-596.

[7]. N. Yazdi, K. Najafi, "An Interface IC for A Capacitive Accelerometer," in *Proc. of IEEE Int. Solid-State*

Circuit Conf. Digest of Technical Papers, San Francisco, CA, 1999, pp. 274-275.

[8]. C. Lu, M. Lemkin, B. Boser, "A Monolithic Surface Micromachined Accelerometer with Digital Output," in *Proc. of IEEE Solid-state Circuit Conf. Digest of Technical Papers*, pp.160-161, San Francisco, CA, 1995.

[9]. Kraft. M, "Closed-loop Digital Accelerometer employing over-sampling conversion," Ph.D. Dissertation, School of Engineering, Coventry University, UK, 1997.

[10]. G. Zhang, "Sensing and Control Electronics for Low-Mass Low-Capacitance MEMS Accelerometer," Ph.D. Dissertation, Dept. of ECE, Carnegie Mellon University, 2002.

[11]. Dan. Simon, *Optimal State Estimation*, WILEY INTERSCIENCE, 2006.

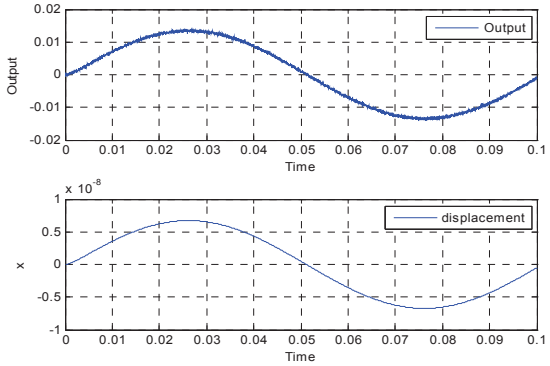

Fig. 7: Open-loop system with 0.1*g* acceleration input

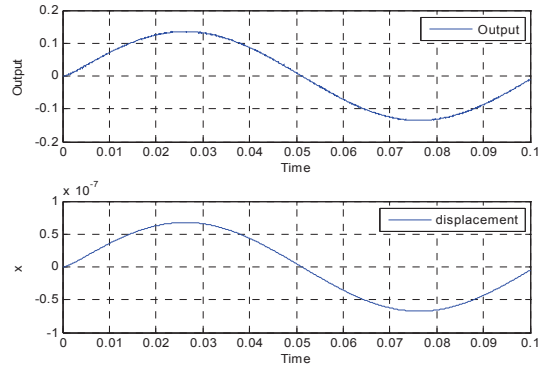

Fig. 8: Open-loop system with 1*g* acceleration input

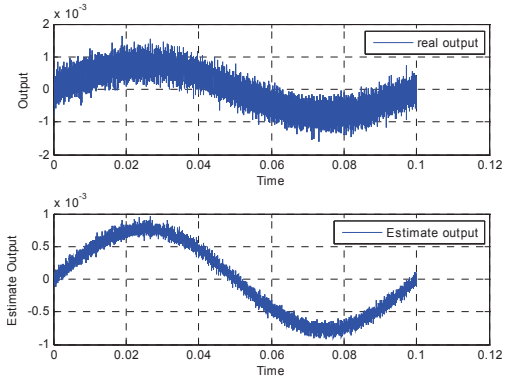

Fig. 9: Actual and estimated voltage outputs with 0.1*g* acceleration input

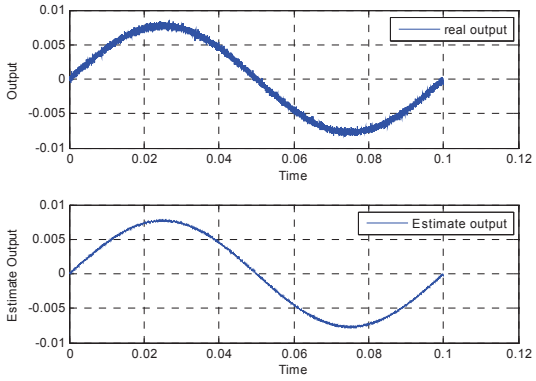

Fig. 10: Actual and estimated voltage outputs with 1 *g* acceleration input

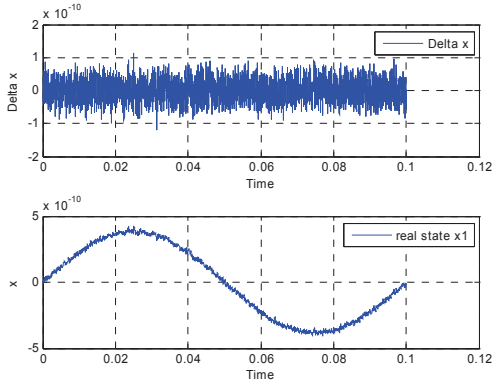

Fig. 11: Actual and estimated displacements with 0.1 *g* acceleration input

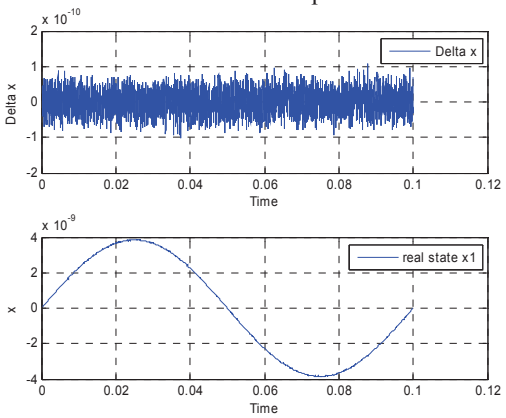

Fig. 12: Actual and estimated displacements with 1*g* acceleration input

Table II: The SNRs and mass' maximum displacements for two different accelerometer systems

Input acceleration' s magnitude	Open-loop		Hybrid EKF based closed-loop	
	Output SNR	Maximum displacement	Output SNR	Maximum displace--ment
0.1*g*	>40 dB	7×10^{-9}m	12 dB	4×10^{-10}m
1*g*	>40 dB	7×10^{-8}m	32 dB	4×10^{-9}m